2D mm-wave imaging based on singular value decomposition

B. Mamandipoor*, U. Madhow#, A. Arbabian*
*EE Department, Stanford University, USA
#ECE Department, University of California, Santa Barbara, USA
{bmamandi, arbabian}@stanford.edu, madhow@ece.ucsb.edu

***Abstract*— In this paper, we develop a systematic framework for two-dimensional mm-wave imaging, based on the singular value decomposition (SVD) of the Helmholtz wave equation under the Born approximation. We identify the degrees of freedom as a function of the geometry of the aperture and the scene, and provide insight into the eigenmodes identified by the SVD. For sparse arrays with number of elements smaller than the degrees of freedom, we propose, and experimentally demonstrate the efficacy of, an eigen-filtered pseudo-inverse algorithm which selects the eigenmodes being imaged.**

***Keywords*— millimeter-wave radar imaging, reconstruction algorithms, imaging eigenmodes, singular value decomposition.**

I. Introduction

Significant recent advancements in silicon processes, RFIC design and low-cost packaging at mm-wave frequencies [1], along with the abundance of available bandwidth (e.g., 14 GHz of unlicensed spectrum between 57 and 71 GHz), offer the possibility of realizing high resolution, low cost and highly integrated sensing and imaging systems. The applications of such systems range from medical imaging, security scanning, and human gesture recognition, to object recognition and scene understanding on moving platforms, such as autonomous vehicles, robots and drones. In this paper, we seek to lay a systematic foundation for short-range two-dimensional (2D) mm-wave imaging, identifying imaging eigenmodes and proposing a new method for image reconstruction based on an SVD of the Helmholtz wave propagation equation.

While SVD techniques have been successfully employed in both optical imaging [2] and MIMO communications [3], these systems involve one-way (transmission-based) propagation, in contrast to the two-way (reflection-based) propagation in radar imaging. The key contributions of this paper are as follows:

- We identify the number of degrees of freedom (DoF) as a function of aperture and scene geometry. While our approach applies to both monostatic and multistatic systems, we restrict attention here to a monostatic system due to space restrictions.
- We provide insight into the nature of the SVD eigenmodes, which are orthonormal basis functions for the electromagnetic waves at the aperture and the scene.
- For imaging with a sparse array with number of elements smaller than the DoF, we propose an *eigen-filtered pseudo-inverse* reconstruction algorithm, which limits the set of eigenmodes contributing to the reconstruction.

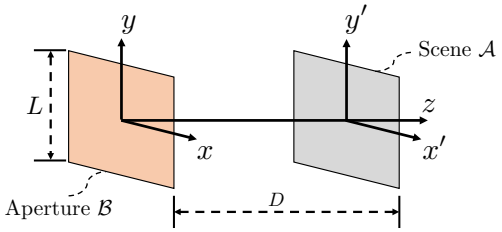

Fig. 1. Geometry of 2D planar imaging system.

- We demonstrate through experimental data that the proposed algorithm is capable of suppressing the "grating lobes" associated with sparse arrays, while reducing the computational cost of the image formation procedure.

II. SVD for the Helmholtz wave equation

Consider the 2D planar imaging geometry depicted in Fig. 1. The scene is located at $z = D$ and is bounded by $\mathcal{A} \subset \mathbb{R}^2$, and the transmitter (Tx) and receiver (Rx) elements are located on an aperture at the origin, and parallel to the scene. The extent of the aperture is denoted by $\mathcal{B} \subset \mathbb{R}^2$. We consider a monostatic imaging array, in which the Tx and Rx elements are co-located (i.e., when the scene is illuminated by a Tx element, only the co-located Rx captures the back-scattered electromagnetic wave). The scene is characterized by the electromagnetic reflectivity function $\gamma(x', y')$, for any point scatterer located at (x', y'). Under Born approximation, the measurement $s(x, y)$ acquired by a Tx/Rx pair located at (x, y) is governed by Helmholtz wave equation for isotropic homogeneous media (simplified by dropping the space attenuation factors), given by

$$s(x,y) = \int_{\mathcal{A}} \gamma(x',y')\xi(x,y,x',y')dx'dy', \tag{1}$$

where

$$\xi(x,y,x',y') \triangleq e^{-j\frac{4\pi}{\lambda}R(x,y,x',y')}, \tag{2}$$

is the space-variant impulse response of the system, and λ represents the signal wavelength. The Euclidean distance between the Tx/Rx pair at (x, y), and the point scatterer in the scene located at (x', y') is denoted by

$$R(x,y,x',y') = \sqrt{(x-x')^2 + (y-y')^2 + D^2}.$$

We now show that the SVD decomposes the Helmholtz wave equation in (1) into multiple parallel and independent

components [4]. It is easy to see that for a bounded aperture and scene, the impulse response ξ is square integrable,

$$\iint_{\mathcal{B}\mathcal{A}} |\xi(x,y,x',y')|^2 dx'dy'dxdy < \infty. \quad (3)$$

Hence, we can invoke the Spectral Theorem [5], and introduce the SVD of the integral operation in (1), by expanding ξ as a weighted summation of eigenmodes,

$$\xi(x,y,x',y') = \sum_{i=1}^{\infty} \sigma_i \phi_i(x,y) \psi_i^*(x',y'), \quad (4)$$

where $(\cdot)^*$ denoted complex conjugate operation. The two sets of orthonormal functions $\{\phi_i(x,y)\}_{i\in\mathbb{N}}$ and $\{\psi_i(x',y')\}_{i\in\mathbb{N}}$ are the singular functions of the system defined over the aperture $\mathcal{B}$ and the scene $\mathcal{A}$, respectively. The associated non-negative weights $\{\sigma_i\}_{i\in\mathbb{N}}$ to each pair of singular functions (ϕ_i, ψ_i) in (4), are known as singular values. We term the triplet of $\{\sigma_i, \phi_i, \psi_i\}$ the i^{th} *eigenmode*. Substituting (4) in (1), gives

$$s(x,y) = \sum_{i=1}^{\infty} \sigma_i \phi_i(x,y) \left\langle \gamma(x',y'), \psi_i(x',y') \right\rangle, \quad (5)$$

where

$$\left\langle \gamma(x',y'), \psi_i(x',y') \right\rangle \triangleq \int_{\mathcal{A}} \gamma(x',y') \psi_i^*(x',y') dx'dy', \quad (6)$$

represents the inner product of the scene reflectivity function, and i^{th} singular function over the scene. Our goal is to use the SVD-based formulation of Helmholtz wave equation in (5) to devise a new image formation algorithm, and to validate our results using measurement data. It is important to note that the sets of singular functions $\{\phi_i(x,y)\}_{i\in\mathbb{N}}$ and $\{\psi_i(x',y')\}_{i\in\mathbb{N}}$ provide orthonormal basis functions spanning the measurements space (i.e., space of $s(x,y)$ functions) and the scene reflectivity space (i.e., space of $\gamma(x',y')$ functions), respectively. Hence the SVD representation in (5) decomposes the overall measurement system into parallel, independent, and non-interfering eigenmodes, where the signal to noise ratio (SNR) of each eigenmode is proportional to its associated squared singular value σ_i^2.

A. Degrees of Freedom

We briefly discuss some of the practical implications of the SVD representation in (5). Given the SVD expansion of the impulse response ξ in (4), it is easy to see that the square integrability in (3), translates to

$$\sum_{i=1}^{\infty} \sigma_i^2 < \infty, \quad (7)$$

that is, the sum of squares of singular values of the system is finite. The inequality in (7) is known as the *sum rule* [2], and indicates that if we order the singular values in a non-increasing order, then

$$\lim_{i\to\infty} \sigma_i^2 = 0. \quad (8)$$

In other words, among the infinitely many eigenmodes in (5), only a finite number are *practically useful*, and they are the ones with a large singular value σ_i, and hence a large SNR [2], [3]. The singular values typically exhibit a step-like behaviour where they are approximately equal up to a certain *threshold*, after which they rapidly decay to zero [2]. This threshold is also known as the *degrees of freedom* (DoF) of the imaging system [4], [6].

In this paper, we skip the derivations of the DoF as a function of the imaging geometry for our 2D reflection-based imaging scenario due to space limitation. See [4] for a detailed DoF analysis for monostatic and multistatic imaging systems, and [7], [8] as example approximations of DoF for 1D transmission-based imaging systems.

B. SVD for a nominal geometry

We consider the following nominal geometry for illustrating our theoretical results and experiments: aperture of 15 cm $\times$ 15 cm, in front of a 2D scene with the extent of 20 cm $\times$ 20 cm. The distance of the aperture and the scene is $D = 30$ cm. The singular values and the eigenmodes corresponding to a certain imaging geometry do not depend on the scene, hence they can be computed offline and later used for image reconstruction after the data acquisition.

Fig. 2 shows the normalized singular values σ_i/σ_{max} corresponding to our nominal imaging geometry, where σ_{max} is the largest singular value of the system. We see that the singular values follow a step-like behavior with a threshold at approximately $DoF \approx 1130$, after which they quickly decay to zero. Fig. 3 shows multiple examples of the eigenmodes at the aperture and the corresponding functions at the scene for our nominal geometry. These orthonormal functions serve as basis functions for the measured electromagnetic waves at the aperture and the scene, respectively. In the next section, we will use these basis functions to introduce a new image formation technique.

III. Pseudo-inverse image formation

Image formation techniques aim to reconstruct the reflectivity function of the scene by solving an inverse scattering problem. In this section, we describe an image formation technique based on the decomposition in Section II. We first approximate the SVD-based formulation of

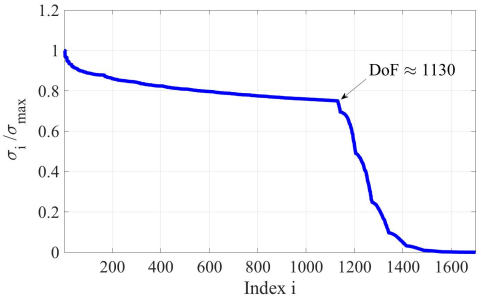

Fig. 2. Normalized singular values corresponding to the nominal geometry.

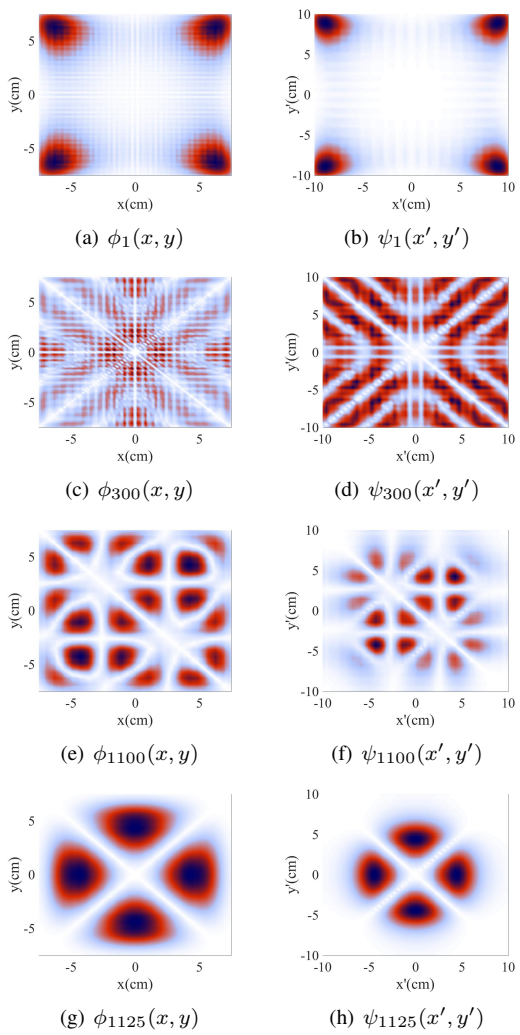

(a) $\phi_1(x,y)$ (b) $\psi_1(x',y')$

(c) $\phi_{300}(x,y)$ (d) $\psi_{300}(x',y')$

(e) $\phi_{1100}(x,y)$ (f) $\psi_{1100}(x',y')$

(g) $\phi_{1125}(x,y)$ (h) $\psi_{1125}(x',y')$

Fig. 3. Magnitude of sample eigenmodes (i.e., basis functions derived from the SVD) at the aperture (left column), and at the scene (right column), for our nominal geometry.

the Helmholtz wave equation in (5) by only including the practically useful eigenmodes:

$$s(x,y) \approx \sum_{i=1}^{DoF} \sigma_i \phi_i(x,y) \left\langle \gamma(x',y'), \psi_i(x',y') \right\rangle. \quad (9)$$

This approximation is known as Truncated SVD (TSVD) [4], [5]. Here we introduce an image reconstruction technique based on computing the pseudo-inverse (PINV) of (9) in order to find the best approximate solution of the inverse scattering problem. The PINV reconstructed image is given by

$$\begin{aligned} \hat{\gamma}_{pinv}(x',y') &= \sum_{i=1}^{DoF} \frac{1}{\sigma_i} \psi_i(x',y') \left\langle s(x,y), \phi_i(x,y) \right\rangle \\ &= \sum_{i=1}^{DoF} w_i \psi_i(x',y'), \end{aligned} \quad (10)$$

that is, the PINV reconstructed image of the scene is derived by computing a weighted summation of the eigenmodes over the scene (i.e. $\psi_i(x',y')$ functions). The weight w_i corresponding to $\psi_i(x',y')$ is derived by

$$w_i \triangleq \frac{1}{\sigma_i} \left\langle s(x,y), \phi_i(x,y) \right\rangle. \quad (11)$$

Next we present PINV reconstruction for a uniform 2D array of monostatic elements.

A. PINV reconstruction using a monostatic array

Consider an $N \times N$ array of monostatic elements, uniformly spaced over the aperture $\mathcal{B}$. The location of $(n,m)^{th}$ element is given by $x_n = (n-1)d$, and $y_m = (m-1)d$, where $d = L/(N-1)$, and $m,n \in \{1,2,\ldots,N-1\}$. The consequence of using a discrete array of Tx/Rx elements for capturing the data is that we only have the value of $s(x,y)$ over a discrete grid. Therefore, evaluating the weights of the PINV image in (11) is carried out by the following summation over the discrete grid of elements,

$$w_i \approx \frac{d^2}{\sigma_i} \sum_{n=1}^{N} \sum_{m=1}^{N} s(x_n,y_m) \phi_i^*(x_n,y_m). \quad (12)$$

Increasing the number of array elements N, provides a more accurate approximation of (11), while increasing the overall SNR.

IV. Experimental Results

In this section we provide experimental results of applying PINV reconstruction technique using an array of monostatic elements. We investigate the effect of the number of array elements on PINV image quality, as well as the choice of eigenmodes used for PINV reconstruction.

A. Experimental setup

Our experimental setup, shown in Fig. 4, is a 60 GHz quasi-monostatic transceiver element with dual high-gain horn antennas, mounted on a mechanical platform used to move the transceiver on a plane parallel to the scene to emulate an array of antenna elements for static scenes. The Tx/Rx antennas are slightly separated but appear to be co-located as viewed from the target. We consider two planar array configurations covering the aperture of size 15 cm $\times$ 15 cm: (1) dense array of 75×75 elements ($d \approx 0.4 \times \lambda = 0.2$ cm), and (2) sparse array of 15×15 elements ($d \approx 2\lambda = 1$ cm). The scene contains copper strips placed on a cardboard at the nominal distance of $D = 30$ cm from the aperture.

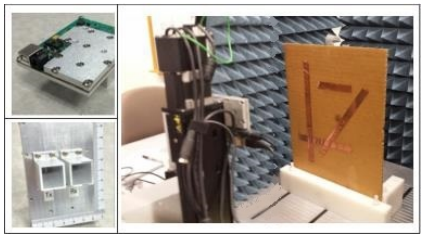

Fig. 4. Experimental setup for emulating a 2D 60 GHz monostatic array using a mechanical platform.

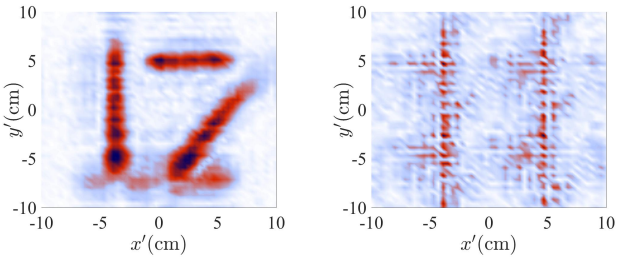

(a) Dense array (b) Sparse array

Fig. 5. PINV-based reconstructed image of the scene $|\hat{\gamma}_{pinv}(x', y')|$, using the entire set of eigenmodes (i.e., with indices in the interval $(1, DoF)$), for the dense and sparse array configurations. Note that applying a standard matched-filter algorithm for image reconstruction using a sparse array leads to a very similar result as the image (b), and is omitted due to space limitation.

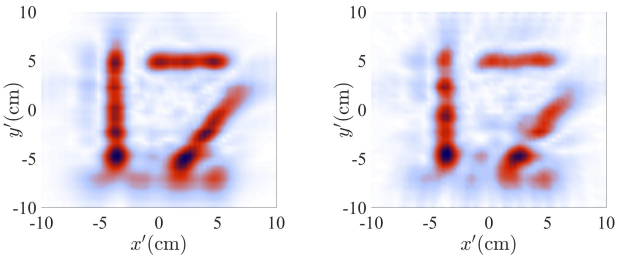

(a) Dense array (b) Sparse array

Fig. 6. PINV-based reconstructed image of the scene after applying a filter in the SVD domain to choose a subset of the eigenmodes within the interval $(1018, 1130)$, for the dense and sparse array configurations.

As we discussed in Section III-A, using a discrete array of elements for data capture leads to an approximate evaluation of PINV weights based on Equation (12), with the quality of approximation directly proportional to the density of array elements. For sparse spatial sampling, the eigenmodes can lose their orthogonality and interfere with each other, leading to poorer reconstruction. Fig. 5 shows the reconstructed images of the scene using the PINV method in (10). We see that the dense array produces a clean and high resolution image, while the sparse array fails to produce an image due to the extreme sub-sampling of the aperture. Specifically, we see that the sparse (sub-Nyquist) array leads to aliasing effects (also known as "grating lobes") that significantly reduces the quality of the image. However, as discussed below, it is possible to get vastly improved imaging performance by examining the eigenmodes under spatial sub-sampling.

B. *Eigen-filtered pseudo-inverse*

In order to suppress the grating lobes in the sparse array, we apply a filter in the SVD domain by choosing a small subset of the eigenmodes for image reconstruction. To this end, we have analyzed the *spatial bandwidth* of the singular functions over the aperture, and have identified those with a *low pass* structure. The intuition behind this choice of functions is that natural scene are often slowly varying in the spatial domain, hence exhibit a low pass structure in the spatial frequency domain. Specifically, we only use 10% of the available eigenmodes within the interval $(1018, 1130)$, most of which have a low pass structure, for computing the PINV in (10). Such an *eigen-filtered* PINV has two main consequences: (i) reducing the interference between the eigenmodes, and suppressing the grating lobes that were generated as a result of sparse deployment of the array, (ii) reducing the computational complexity of the PINV image formation procedure and speeding up the algorithm drastically. For example, for the filter implemented in this subsection, the speed of the algorithm has increased by a factor of 10.

Fig. 6 shows the result of PINV-based reconstruction technique after applying the eigen-filter in the SVD domain. We see that constructing the images using this partial sum leads to a significant improvement in the image corresponding to the sparse array by suppressing the grating lobes, while reducing the computational cost of the image formation procedure for both dense and sparse array configurations.

V. Conclusions and Future work

In this paper, we investigated 2D mm-wave imaging based on SVD analysis, and demonstrated the applicability of this framework for suppressing grating lobes associated with sparse imaging arrays through experimental data. The proposed SVD approach offers new criteria for designing non-uniform antenna arrays: for example for a given collection of eigenmodes, we can choose the location of antenna elements such that the weights of PINV image evaluated over the non-uniform discrete grid best approximates the weights over the continuum in (11). Moreover, SVD framework provides an interesting opportunity for *designing eigen-filters* based on the available eigenmodes.

Acknowledgement

This research was supported in part by the National Science Foundation under grants CNS-1518812 and CNS-1518632.

References

[1] A. Arbabian, S. Callender, S. Kang, M. Rangwala, and A. M. Niknejad, "A 94 ghz mm-wave-to-baseband pulsed-radar transceiver with applications in imaging and gesture recognition," *IEEE Journal of Solid-State Circuits*, vol. 48, no. 4, pp. 1055–1071, 2013.

[2] R. Piestun and D. A. Miller, "Electromagnetic degrees of freedom of an optical system," *JOSA A*, vol. 17, no. 5, pp. 892–902, 2000.

[3] E. Torkildson, U. Madhow, and M. Rodwell, "Indoor millimeter wave mimo: Feasibility and performance," *IEEE Transactions on Wireless Communications*, vol. 10, no. 12, pp. 4150–4160, 2011.

[4] B. Mamandipoor, A. Arbabian, and U. Madhow, "Geometry-constrained degrees of freedom analysis for imaging systems: Monostatic and multistatic," *CoRR*, vol. abs/1711.03585, 2017. [Online]. Available: http://arxiv.org/abs/1711.03585

[5] M. Bertero and P. Boccacci, *Introduction to inverse problems in imaging*. CRC press, 1998.

[6] G. T. Di Francia, "Degrees of freedom of an image," *JOSA*, vol. 59, no. 7, pp. 799–804, 1969.

[7] R. Pierri and F. Soldovieri, "On the information content of the radiated fields in the near zone over bounded domains," *Inverse Problems*, vol. 14, no. 2, p. 321, 1998.

[8] R. Solimene, M. A. Maisto, G. Romeo, and R. Pierri, "On the singular spectrum of the radiation operator for multiple and extended observation domains," *International Journal of Antennas and Propagation*, 2013.